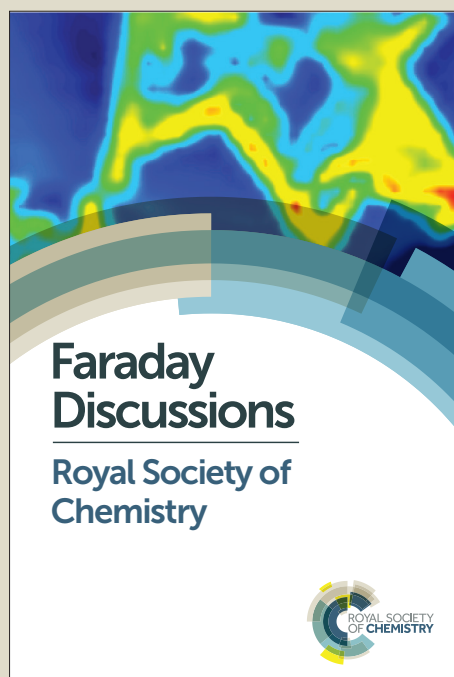# Faraday Discussions

Accepted Manuscript

This manuscript will be presented and discussed at a forthcoming Faraday Discussion meeting.
All delegates can contribute to the discussion which will be included in the final volume.

Register now to attend! Full details of all upcoming meetings: http://rsc.li/fd-upcoming-meetings

Faraday Discussions

Royal Society of Chemistry

ROYAL SOCIETY OF CHEMISTRY

www.rsc.org/faraday_d

Journal Name

ARTICLE

Designing disordered materials using DNA-coated colloids of bacteriophage fd and gold

Z. Ruff,[a,†] S. H. Nathan,[a,†] R. R. Unwin,[a,†] M. Zupkauskas,[a] D. Joshi,[a] G. P. C. Salmond,[b] C. P. Grey, [c] and E. Eiser[a,d*]

DNA has emerged as an exciting binding agent for programmable colloidal self-assembly. Its popularity derives from its unique properies: it provides highly specific short-ranged interactions and at the same time it acts as a steric stabilizer against non-specific van der Waals and Coulomb interactions. Because complementary DNA strands are linked only via hydrogen bonds, DNA-mediated binding is thermally reversible: it provides an effective attraction that can be switched off by raising the temperature only by a few degrees. In this article we introduce a new binary system made of DNA-functionalized filamentous fd-viruses of ∼880 nm length with an aspect ratio of ∼100, and 50 nm gold nanoparticles (gold-NPs) coated with the complementary DNA strands. When quenching mixtures below the melt temperature T_m, at which the attraction is switched on, we observe aggregation. Conversely, above T_m the system melts into a homogenous particulate `gas'. We present the aggregation behavior of three different gold-NP to virus ratios and compare them to a gel made solely of gold-NPs. In particular, we have investigated the aggregate structures as a function of cooling rate and determine how they evolve as function of time for given quench depths, employing fluorescence microscopy. Structural information was extracted in the form of an effective structure factor and chord length distributions. Rapid cooling rates lead to open aggregates, while slower controlled cooling rates closer to equilibrium DNA hybridization lead to more fine-stranded gels. Despite the different structures we find that for both cooling rates the quench into the two-phase region leads to initial spinodal decomposition, which becomes arrested. Surprisingly, although the fine-stranded gel is disordered, the overall structure and the corresponding length scale distributions in the system are remarkably reproducible. Such highly porous systems can be developed into new functional materials.

Introduction

Since the introduction of grafting dense coatings of short single-stranded (ss) DNA on to nanoparticles [1, 2], it has become possible to direct colloid-colloid self-aggregation. By barcoding different colloids, specific binding rules could be introduced to enable hierarchical colloidal aggregation, which was not possible with standard non-specific interactions. The main focus was on building colloidal crystals[3-6] with prescribed order for the development of photonic applications. The sharp melt transition of DNA-coated colloids, typically only 1-2°C wide, made forming colloidal crystals difficult. Instead these systems would form dynamically arrested gels when quenched into the two-phase region[7, 8]. Furthermore, the narrow melt region made annealing aggregates into equilibrium ordered solids almost impossible[6].
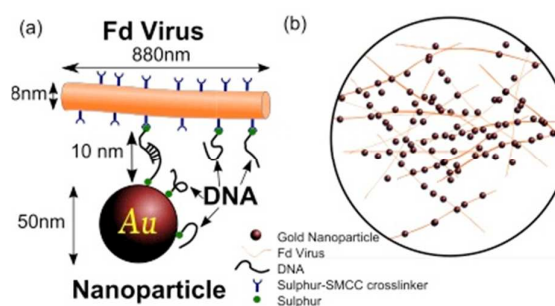
Fig. 1 Schematic of the system. (a) Gold nanoparticles are attached reversibly to fd viruses (filamentous ssDNA bacteriophages) via pairs of complementary DNA strands. (b) Cartoon, depicting the expected local network structure of viruses and nanoparticles in a kinetically arrested state.

a. Cavendish Laboratory, University of Cambridge, JJ Thomson Ave, Cambridge, CB3 0HE, UK. E-mail: ee247@cam.ac.uk.
b. Department of Biochemistry, University of Cambridge, Tennis Court Rd, Cambridge, CB2 1QW, UK.
c. Department of Chemistry, University of Cambridge, Lensfield Road, CB2 1EW, Cambridge, UK.
d. BP Institute, Bullard Laboratories, Madingley Rd, CB3 0EZ Cambridge, UK.
† equal contributions.
Electronic Supplementary Information (ESI) available: video SV1, SV2, SV3 and SV4.

However, many colloidal systems in nature such as photonic colours in birds and insects[9, 10] and applications such as paints, random lasers[11], ceramics[12] and battery materials[13, 14] are inherently disordered. This makes the structural and dynamic study of colloidal gels and glasses particularly relevant. A rich literature on the dynamic behaviour of very dense hard sphere

ARTICLE

suspensions in the glassy or super-cooled phase has led to a good understanding of these systems[15-18]. In contrast, the aggregation and gelation dynamics of low-density suspensions of colloids interacting via van der Waals or short-range depletion interactions is less established. In recent years, the depletion-driven aggregation in low-density systems of spherical colloids has been studied both in experiments and in simulations[19-23]. In all these systems, the overall range and depth of attraction are fixed during a quench into the two-phase region[24]. Here we show that, similar to colloidal aggregation induced by depleting polymers, single and mixed DNA-coated colloidal suspension mixtures initially exhibit spinodal decomposition when quenched, followed by kinetic arrest. However, very different disordered structures can be achieved depending on the quench rate.

Previously we have shown that we can exploit the selectivity and strength of the short-ranged interactions to form bigels composed of two independent porous inter-percolating gels made of spherical sub-micron particles[25-27]. In order to develop new, high surface area, functional materials with tuneable porosity made with a variety of colloidal materials, we introduce a new system, namely a binary mixture of semi-flexible rods and nanoparticles. In our model system, monodisperse filamentous fd-viruses were used as the semi-flexible rods. Short ssDNA (S) was attached to the side-coat proteins of the virus[28]. The complementary ssDNA (S') was grafted to gold nanoparticles (gold-NPs) as shown in the schematic in Fig. 1 and the DNA sequence is given in the Experimental section. Fluorescence microscopy was used to monitor the time evolution of the gel structures for different quench rates and depths.

Results and Discussion

### Virus and Au-nanoparticle gels – fast versus slow quench

We studied gold-NP mixtures with three different number ratios (R_{GV}) of gold NPs to virus particles. The volume fraction of gold colloids, ϕ_{gold}, was 0.1% in all samples. Systems with R_{GV} = 2.5, 5 and 10, were studied, along with a control sample comprising only gold-NPs, for which half of the spherical particles were coated with S DNA and the other with S'. For details see the Experimental section. Fluorescence microscope images were then obtained from these samples before heating, after heating, and after a controlled quench to room temperature (Fig. 2). The aqueous solvent is fluorescently labeled and hence the regions containing a high concentration of the gold colloids are visible as dark patches in the microscope images. Although the fd-virions are almost one micrometer long they are too thin to be visible in optical microscopy. Individual gold-NPs are also too small and highly diffusive to be visible. Images acquired of the samples in the melted or gas phase, showed that the viruses and the gold-NPs were fully dispersed and no sedimentation was observed (Fig. 2(c)). In the right-hand pan of Fig. 2, we show the structure factors corresponding to the real-space images in the left-hand pane. Very different structures were observed before (Fig. 2(a)), and after the melting process Fig. 2(b)). These structures

will be referred to as *'open'* and *'homogenised'*, respectively. As discussed in the next paragraphs, the differences in morphology arise from the different cooling protocols from the uniform, high-temperature phase.

The open structures were obtained for all three sample ratios, when the samples were quenched from 60°C (the temperature used during the preparation of the cuvettes containing the samples, outside the microscope) to room temperature (RT) (the initial temperature inside the microscope). Since RT is well below the DNA melt temperature, T_m ($\approx$ 42°C), the rods and spheres start to aggregate and the suspension can undergo macroscopic phase separation. The rapid loading of the sample cells in the microscope resulted in a fast cooling process, as illustrated in Fig. 3. By subsequently heating the sample inside the microscope to 50°C for a sufficiently long time, we return the colloids to the non-aggregated 'gas' phase. We can quench the sample back to RT to obtain a more homogenous, fine-stranded gel structure (Fig. 2(b)). Gelled aggregates settle to the lower part of the sample chamber, leaving an aggregate-free top layer. Using a Peltier-stage for controlled heating and cooling, we could reproduce this characteristic fine-stranded gel structure for many melting and cooling cycles around the melt temperature.
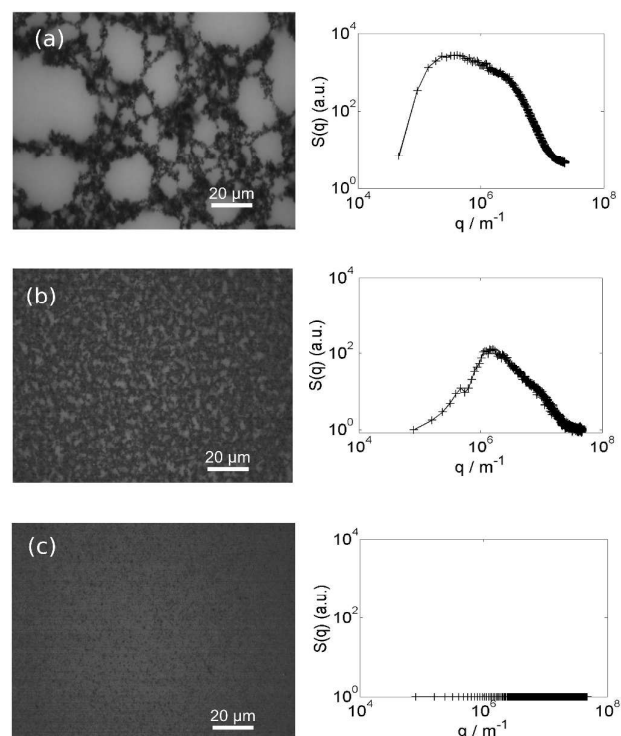
Fig. 2 Epifluorescent microscope images and the corresponding effective structure factor showing the difference in structure for (a) rapidly cooled (open), (b) slowly cooled homogenised and (c) melted virus-colloid structures, with their associated $S(q)$. A gold-NP to virus ration R_{GV} = 5 and gold-NP volume fraction, ϕ_{gold} = 0.1%, were used. The images shown in (a) and (b) were obtained at RT while (c) was obtained at 50°C. The light regions show the fluorescently labelled aqueous phase.
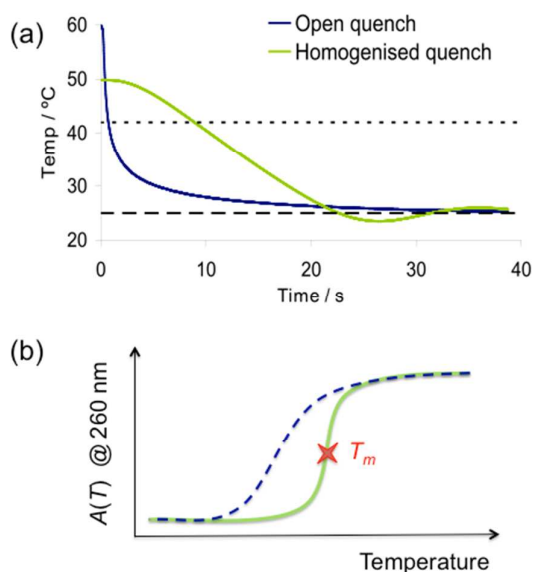
Fig. 3 (a) Curves showing the difference in quench profiles between the homogeneous and open structures. When the temperature through T_m (dashed line), the open structure obtained for the fast cooling rate of -12°C/s, and the homogenized one for the slower cooling rate of -1.5°C/s. (b) Schematic melt curves. The solid line corresponds to equilibrium cooling and heating curves, while the dashed line indicates a hypothetical out of equilibrium cooling curve.

By comparing the results for the quench rates, it becomes apparent that the fast quench resulted in an approximately exponential time dependence of the temperature, while during the slower controlled cooling rates the T-t relation was nearly linear for temperatures between T_m and RT (Fig. 3(a)). In order to understand the difference in the resulting open and more homogenised gel structures we need to consider the rather slow process of DNA hybridisation that requires the correct zipping into the desired duplex, which is observed in DNA melt-curve measurements. Only for sufficiently slow cooling or heating rates, no hysteresis in the hybridisation curves is observed. A schematic cooling curve is drawn in Fig. 3(b). On rapid cooling, the fraction of faulty base pairs is high. This effect leads to a lower apparent melt temperature, reflecting that the structure that has formed is, on average, less stable than a structure that is formed under equilibrium. Rapid cooling therefore results in a shifted (and broadened) melting curve (see Fig. 3(b)). At first sight, the structures reported in Figs. 2(a) and 2(b) seem incompatible with the assumption of spinodal decomposition, as a shallow quench would allow the evolution of longer wavelength instabilities than a deep quench. However, one should bear in mind that what we observe is the 'aged' structure. We hypothesize that in the rapid quench, many small clusters form. These clusters can still diffuse and will aggregate into the morphology shown in Fig. 2(a). In fact, the thickness of the (dark) filaments in Fig. 2(a) is compatible with the assumption that it consists of smaller clusters. Additional evidence for this scenario comes from the chord analysis to be discussed in the context of Fig. 4. In contrast, the slow quench will result in much larger clusters that diffuse much more slowly and, eventually, get structurally arrested.

Further evidence for the above scenario comes from an analysis of the structure factors $S(q)$ plotted in Fig 2. As expected $S(q)$ is featureless when the sample is in the gas phase. However, for the slow quench (Fig. 2(a) and (b)) a well-defined peak in $S(q)$ appears, as one would expect for (arrested) spinodal decomposition. In contrast, for the fast quench (Fig. 2(a)), the peak in $S(q)$ is unusually broad, compatible with the assumption that spinodal decomposition is followed by aggregation of the primary clusters.

From our results for $S(q)$ we can estimate an average length scale L_o defined through $\sum qS(q)/\sum S(q) \equiv q_{ava} \equiv 2\pi/L_0$, where q_{ava} denotes the average scattering vector. Using this definition, we can estimate an average length scale $L_o = 3.4$ μm for the open, and $L_h = 1.3$ μm for the homogenised structure, of a gold-NPs to virus ratio $R_{GV} = 5$ and a gold colloid volume fraction $\phi_{gold} = 0.1\%$. We also analysed the structure factor of the open structures of samples with the same ϕ_{gold} but different R_{GV} (see Table 1). We observe that L_o becomes smaller as the number of colloids per fd-virion increased. This makes sense when interpreting the gold-NPs as linkers that can bind virions together. The larger the number of gold NPs, the higher the maximum effective coordination number of the virions, in analogy to spherical colloids with varying number of sticky patches[30]. Similarly, our spheres with isotropic binding potential can only bind maximally 12 other spheres but because of the stick-conditions provided by the DNA the effective coordination number will be much smaller, reflecting the larger L_o and λ_{oa}.

Ratio gold-NPs to virus R_{GV}	$L_o(S(q))$ /μm	λ_{oa} /μm	λ_{op} /μm
		aggregates	pores
2.5	7.4	4.36	11.01
5	5.4	2.98	14.57
10	3.5	1.77	23.70
control	10.5	7.41	9.82

Table 1 Length scales for the open structured gels with different rod-sphere ratios, as well as a sphere-sphere control sample following a fast quench. The characteristic length scale of the open structure, defined as $L_0 = 2\pi/q_{ava}$, were obtained from $S(q)$. From chord analysis (Fig. 4) the decay lengths $\lambda_{oa,op}$ of the aggregates and the pores are given respectively. The same gold-NP volume fraction $\phi_{gold} = 0.1\%$ was used in all samples.

Using UV-vis spectrometry we estimated an S DNA grafting density on the virus to be roughly 160 strands per virion[28] rendering the rod diameter roughly 12 nm compared to the 'bare' diameter of 6-8 nm in the solvent's ionic strength used. The gold-NPs carry a much denser S' DNA coating. Hence the 50 nm large gold-NP can bind several fd viruses (if available). In all our experiments on NP-virus mixtures, the number of NPs per virus is larger than one (allowing each virion to bind at least two others but most likely many more) and hence, below T_m the fd virions should always be able to form percolating structures. However, as the volume fraction of virions is quite low, the percolating structures cannot be uniform. The initial

ARTICLE Journal Name

non-uniformity emerges during spinodal decomposition. As the driving force for spinodal decomposition is larger for the systems with large R_{GV}, we expect that the wavelength of the maximally unstable density fluctuations, and hence L_o, is shortest for large R_{GV}. Further coarsening is then arrested by percolation and this again will happen earlier for large R_{GV}.

In conjunction with studying the structure factor, we performed a chord distribution analysis (see section Computational Methods) on the open structures. The resulting histograms (Fig. 4) can be fitted using an exponential with characteristic lengths of $\lambda_{0a} = 4.36$ μm, 2.98 μm and 1.77 μm for R_{GV} = 2.5, 5 and 10 respectively. The values obtained from chord analysis are consistently smaller than L_o, which is not surprising, as the chord analysis and $S(q)$ do not measure the same quantity. Nevertheless both measurements show the same tendency. We note that for a heterogeneous system consisting of two uniform phases, the ratio of the chord lengths is equal to the volume fractions occupied by the two phases. If we interpret the data in Table 1 in terms of a two-phase system, we must conclude that, at constant height (our microscopy images, probe a cross section of the system), the system with R_{GV} =10 has an effective gel volume fraction of 7%, whereas the system with R_{GV} =2.5, has a volume fraction of 28%. This suggests that the system with R_{GV} =2.5 can sediment much more than the system with R_{GV} =10. We will come back to this point later.

The length scales present in the $S(q)$ peak were obtained by averaging over the entire sample hence including aggregates and pores. The chord analysis technique allows us to separate these two phases. This difference will be further discussed for the homogenized samples.
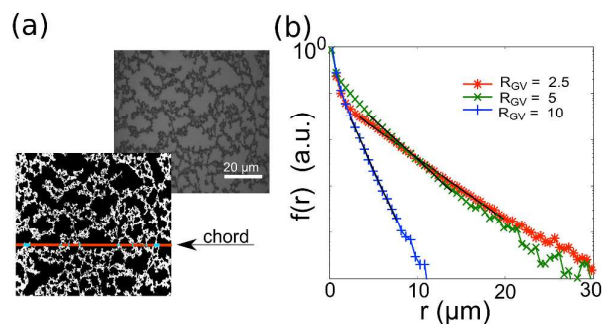
Fig. 4 Chord distribution analysis of open structured gels. (a) A fluorescent image (back) of a sample with colloid to virus ratio of 2.5 was binarized (front). Horizontal and vertical chords are then drawn through the image. (b) The resulting histograms of the distribution of lengths *f(r)* passing through the gel phase (light) and the 'empty liquid' (dark – not shown in the histogram) are shown for all three gold colloid to virus ratios. The fitted solid lines followed an exponential decay with characteristic length λ_{oa} - respective values are plotted in Table 1.

We also measured a characteristic chord length for the control sample made of the same 50 nm large gold-NPs, where half were coated with S and the other half with S' DNA (details are given in the Experimental section). Keeping the gold-NPs' volume fraction at $\phi_0 \approx 0.1\%$, we obtained a $\lambda_{0a} \approx 7.4$ μm for

the open structure, which is considerably larger than that of the virus-colloid structure not only for the fast quench but also for the homogeneous one as we will see later. Similarly, we obtain a larger L_o = 10.5 μm from the $S(q)$ peak maximum. Note that due to the different geometry of the contact region between two spheres to that between a sphere and thin rod, the melt temperature of the pure gold-NP system is increased to $T_m \approx 55°C$.

Structural evolution as function of quench depth

Using the controlled temperature quench from the gas phase to below T_m, we also studied the time evolution of the emerging 'homogenised', phase-separated samples as a function of quench depth. For the time evolution study, we cooled the well-homogenized samples to a given temperature below T_m following the intensity of the emerging peak of the systems structure factor, which we define as $S(q_{max}, t)$. For each quench temperature we first homogenized the sample by heating it to the gas phase. $S(q)$ was calculated from fluorescent microscope images recorded at 20s intervals after the quench. In Fig. 5 such a time evolution is presented for a sample with R_{GV} = 5. Supporting videos and corresponding $S(q, t)$ for the NP-virus system and the control sample are provided as supporting videos SV1 and SV2.

Two important observations become apparent. Firstly, in $S(q)$ the growing structural peak only becomes visible after roughly 20 s, which means that during the growth phase, the temperature of the sample is already at the target temperature. Secondly, the intensity of the emerging structural peak increases until reaching a plateau, while remaining centred about a characteristic wavevector $q_{max} = 1.27 \times 10^6$m, corresponding to a characteristic length scale of about 5 μm. The rather constant position of q_{max} reflects the fact that the sample undergoes a spinodal phase separation, in which the longest characteristic wavelength grows fastest, but no subsequent coarsening occured: the density fluctuation with the characteristic wavevector q_{max} grows until gelation arrests further coarsening of the aggregates, which is marked by the plateau.

In addition we observe the transition from a completely fluid sample with no structural peak at 44°C to the onset of gelation, which we identified to be at $T_m \approx 42°C$. As can be seen in Fig. 5(b) when dropping just to this critical point the peak in the structure factor already shows evidence for demixing, and indeed, a video recording (see supporting video SV1 and SV2) clearly shows clusters forming, even though the sample as a whole still seems to be fluid-like. We speculate that the incipient phase separation at 42°C is due to the heterogeneity in the NP-virion interaction (SV1).
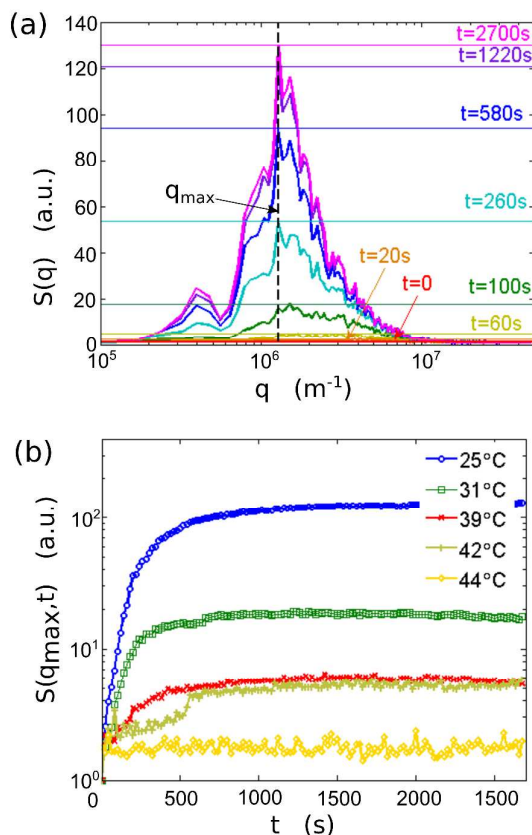
Fig. 5 (a) Time evolution of the structure factor $S(q)$ for a gold-NP-virus sample quenched to 25°C leading to a homogenized structure; R_{GV} = 5. The wavevector q_{max}= 1.27×10^6 m^{-1} of the main peak is marked by the dashed vertical line. The times are measured from the start of the cooling ramp. (b) The height of the maximum of the structure factor over time for various quench-depths for the same rod-sphere gel as in (a) – the $S(q_{max}, t)$ was extracted from fluorescent images taken in the middle of the sample every 20 seconds.

It is surprising that the wavelength of the maximum instability at this temperature is the same as that at lower quench temperatures because a Cahn-Hilliard-style analysis would suggest that the wavelength of the dominant instabilities should grow as the temperature approaches the spinodal from below. At 39°C most of the images show larger clusters and a clearly arrested phase in form of the peak in $S(q)$ and the plateau. Reheating back into the gas phase and then cooling even further to 39°C shows that more of the gel phase of a characteristic length scale is formed (SV2). Comparing the slopes of the increase of $S(q_{max}, t)$ also suggest that the phase separation process becomes faster as we cool deeper into the two-phase region, but the overall structure of the fine-stranded gel does not change much. This may be interpreted in terms of the finite attractive interactions provided by the DNA hybridization, which will be of the order of tens of $k_{B}T$, k_{B} being the Boltzmann constant. As the melt transition region is rather narrow (only a few degrees) the full attractive potential is reached already a few degrees below T_m. Hence it is only the entropic term that provides lowering of the systems Gibbs free energy upon further cooling.
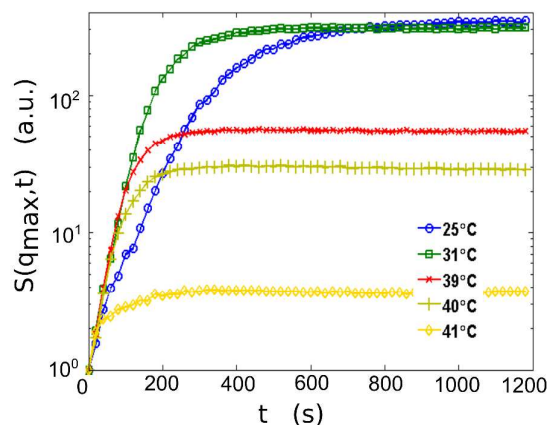

Fig. 6 Time evolution of the structure factor maximum $S(q_{max}, t)$ for the control sample made of only gold-NPs; $\phi_0 \approx 0.1\%$. The melt temperature of this system was at about 44°C.

Following the evolution of $S(q_{max}, t)$ for different quench depths for the control sample of a pure gold-NP gel with $\phi_0 \approx$ 0.1%, we observe a very similar behaviour: while q_{max} remains constant, the corresponding intensity plateaus after a few minutes (Fig. 6). Supporting videos SV3 and SV4 show $S(q, t)$ for quench temperatures from 60°C to about the melt temperature $T_m \approx 55$°C and to 48°C.

Finally, we also performed a chord analysis on all of the homogenized samples for the different quench depths, both after 400 s when $S(q_{max}, t)$ was still growing, and after 1200 s when the plateau region was reached (Fig. 7). Similar to the gelled open structure, the homogenized samples also show an exponential length distribution with characteristic decay lengths λ_{ha}. However, unlike the open and homogenized structures of the control sample, the gelled gold-NP virus structures seem to display two different decay length scales. Both are listed in Table 2. In Fig. 7 we present typical chord analysis results for a sample with R_{GV} = 5, showing the different regimes in the aggregates. However, we stress that, owing to the delicate measurements, large variations in the chord analysis from one set of samples to another need to be considered. Nevertheless, these short length scales, which are roughly a third of the length of the semi-flexible fd-rods, do suggest that the stiffness of the rods combined with the tendency for the gold-NPs to bind as many rods as possible influence the overall gel structure of the system. In contrast, the gold-NP gels only made of spherical 50 nm large particles always show a single decay length λ_{ha}, similar to gels made of DNA-functionalized 500 nm polystyrene spheres, which we studied earlier[26].

homogenized samples	time after quenching /s	λ_{ha} /µm		λ_{hp} /µm
		aggregates		pores
R_{GV}		short lengths	long lengths	
2	400	0.37	4.03	4.09
5	400	0.42	3.20	3.75
10	400	0.36	3.76	2.68
Control	400	1.89	1.95	3.19
2	1200	0.41	4.41	4.74
5	1200	0.39	4.09	3.02
10	1200	0.27	5.25	2.53
control	1200	-	5.18	3.89

Table 2 Characteristic chord lengths extracted from fluorescent microscope images of samples with different gold-NP to virus ratios and control samples, all quenched from 50°C to RT. The given length sales are obtained from averages of 4-5 images from different regions in the 1cmx1cm large sample, but the same height above the bottom surface.
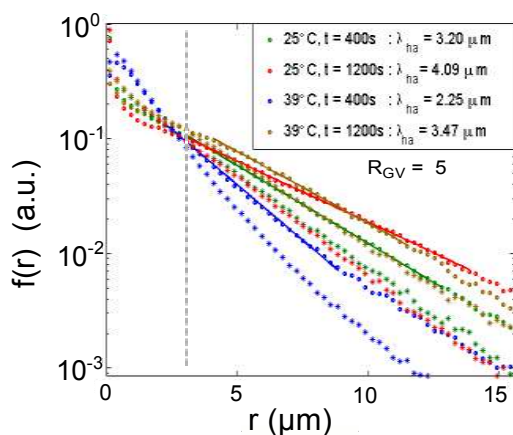
Fig. 7 Chord distribution analysis of a homogeneous fine-stranded gel made of fd-rods and gold-NPs. The distributions for the aggregates are the lines with the solid fitted curves, while the non-fitted data represent the corresponding pore distributions. The vertical dashed line marks the divide between the long decay lengths λ_{ha} (right) and the short ones (left).

Further we note a significant difference between the open and closed aggregate structure for the different R_{GV} values. While the typical long length scales for the homogeneous aggregates are all very similar with 4-5 µm for all three gold-NP to virus ratios they do show significant changes in the open structure. This supports our earlier hypothesis that the very fast quench results in open structures due to the out-of-equilibrium hybridization of DNA, which leads to initially weaker bonding enabling loosely bound particles to detach and reattach onto larger aggregates. This is further supported by the same tendencies for the chord distribution of the pores.

Summarizing our results we demonstrate that the quench rate into the two-phase region governs the aggregation dynamics of DNA-functionalized colloids, as equilibrium DNA hybridization requires finite times. This is very different to colloid-polymer systems in which the depth (strength) of the short-ranged interactions are fixed throughout the quench for a given depleting polymer concentration[18]. The strength of the short-ranged attraction between particles with complementary ssDNA will be initially reduced due to faulty binding events allowing particles to unbind and rearrange leading to an open gel structure. However, when cooled down sufficiently slowly, the maximum attractive well is attained fast enough leading to the more homogenised fine-stranded gel. Using both time dependent structure factor and chord-distribution analysis on 2D fluorescent images, we were able to study these open and homogenized gel structures. Both techniques allowed us to determine that the segregation mechanism is initially due to spinodal decomposition in all cases, which is subsequently dynamically arrested. It is remarkable that the controlled slower cooling reproducibly led to a self-similar homogenized structure with what we call 'designed disorder'. Furthermore, while the $S(q,t)$ measurements provide an excellent tool to follow the dynamics of the aggregation into an arrested state, chord analysis provided us with further information on the aggregate and 'empty liquid' phase separately, giving insight into the dependence on the systems composition for both the rod-sphere and the pure sphere-sphere system.

Finally we note that, unlike sphere-sphere colloidal gels that aggregate in the same way for all sizes between 10nm and a few micrometers, the aggregation behaviour of the rod-sphere system does depend on the size and concentration ratio of the two. In our case we used 50 nm large particles and 880 nm long and 6-8 nm thick semi-flexible rods. When using 500 nm or larger DNA-functionalized spherical colloids we no longer observed significant aggregation in the presence of many more rods per colloids (data not shown here). This is most likely due to the semi-flexible nature of the virions; the gain of hybridization free energy per SS' pair is of the order of 10 k_BT. Hence, the energy to bend the fd-virion will be smaller than the gain from this binding energy provided we have enough ssDNA grafted to the virion. Therefore the viruses will 'wrap' around the colloids inverting the initial ssDNA coating into a complementary coating. The resulting fd-wraped colloids cannot bind to each other, or only weakly if a virus bridges two colloids.

Experimental

Materials and methods

DNA strands were purchased from Integrated DNA Technologies. The sequences were modified from previously published work and had the following structure: 5'(15T)-(binding sequence)-(thiol)3'. The 15 thymine (T) bases are used to increase the entropy of the system by increasing the volume the sticky end can explore around the colloids. Two complementary binding sequences were designed based on minor modifications of a previously published sequence by the

Gang group[4]: they are denoted S for 5'CCA ATC CAA T3' and S' for 5'ATT GGA TTG G3', with S DNA being attached to the fd viruses and S' DNA to the gold nanoparticles.

Virus functionalization

The filamentous fd-virion is about 880 nm long and has a diameter of 6-8 nm. Its capsid coat is made of approximately 2700 copies of the gp8 coat proteins whose NH_2 terminus is pointing outwards[31]. DNA was covalently linked to these gp8 major-coat proteins using a slightly modified protocol developed by Unwin et al.[28], which also describes the growth and purification of fd viruses. An amount of concentrated fd stock solution was diluted into 10mM 4-(2-hydroxyethyl)- 1-piperazineethanesulfonic acid buffer (HEPES buffer, Sigma-Aldrich) at pH 7.0 to make 0.5mL of fd solution at a concentration of 0.25 mg/mL. To this solution, 0.5 mg of sulfosuccinimidyl-4-(N-maleimidomethyl) cyclohexane-1-carboxylate (sulfo-SMCC, Pierce) was added and mixed thoroughly; the mixture was then left to sit at room temperature (RT) for 1 hour in order to functionalize the fd major-coat proteins with thiol-reactive maleimide groups (Fig. 1). At the end of the hour, the fd-SMCC solution was twice desalted using desalting columns (40 kDa MWCO Zebra, Thermo Scientific), in order to remove spent reactants and any remaining cross-linker. Then 20 nM of thiolated S DNA was suspended in 100 μL of phosphate buffer and 100 μL of a 100mM DTT stock solution and is left to react for one hour. The activated thiolated DNA is purified using size elution chromatography (Illustra NAP-25, GE Lifesciences) equilibrated with phosphate buffer and eluted.

To the S DNA solution, 0.25ml of the activated fd solution is added and the total mixture brought up to a salinity of 200mM using 2M NaCl phosphate buffer (Sigma-Aldrich). Due to changes in volume incurred by the desalting process the final mixture of activated fd and thiolated DNA is 1.02ml with an fd molarity of 3.74nM. The mixture is left to sit at room temperature for 2 hours and then is dialysed (100kDa MWCO Spectrum Labs Float-A-Lyzer) against 10-mM Tris-EDTA buffer solution (TE, Sigma-Aldrich) in a refrigerator overnight. The resulting dialysed sample is then collected and stored at 4°C.

Gold nanoparticle functionalization

Citrate capped gold nanoparticles were purchased (Nanocomposix) at a concentration of .05 mg/ml. Sodium dodecyl sulphate (.01%, Sigma-Aldrich) was added to 10ml of gold nanoparticle solution and the suspension was concentrated to 1.0 mg/ml before adding 25nM of activated thiol-functionalized DNA in 10mM phosphate buffer (Sigma-Aldrich). Subsequently, 2M NaCl was added in a stepwise manner to bring the final salt concentration of the solution to 0.5 M[32]. After incubating overnight, the DNA functionalized gold nanoparticle suspension was then washed three times with phosphate buffer, before transferring the nanoparticles to 10mM TE buffer.

Mixing Process

188 μg of gold colloids coated with S' are concentrated from the stock solution (ϕ =0.025 %) by centrifuging (17,000g for 30 minutes). After each spin, as much supernatant as possible is removed with a minimum loss of colloids. This process is repeated until less than 5μL of solution remains (ϕ > 0.2%).

To the DNA-nanoparticle solution, a DNA functionalised fd suspension is added to achieve the required number ratio of viruses to colloids and mixed gently. 0.3 μg of fluorescein sodium salt (Sigma-Aldrich), a fluorescent dye (494/521 nm), is added for inverse staining of the samples, and further TE buffer and NaCl are added to bring the sample up to 10 μL with 50mM salt to screen the negative charge of the phosphate backbones on complementary strands of DNA. The sample is then heated to 60°C for 3 minutes, and finally gently mixed with a vortex.

Sample chambers

Sample chambers were prepared by forming a wedge between a cover slip (18x18x0.15mm) and a standard glass slide, using another, identical, cover slip as a spacer. One edge of the cover slip was glued to the glass slide using Norland Optical Adhesive, while the opposite edge rested on the spacer, which was placed directly on the glass slide. After the glue was allowed to spread via capillary action across the whole of the joint between the glass slide and the cover slip, the epoxy was set using UV light.

To prevent colloids from sticking to the chamber walls, the hydrophobicity of the sample chamber surfaces was increased using a previously published protocol[25]. Before chamber construction, both the glass slide and coverslips were washed with Hellmanex and 3M NaOH. The assembled chamber also was treated with oxygen plasma immediately before loading the sample. To avoid aggregation of the suspension during sample loading, both the sample chamber and sample were heated to 60°C. After sample loading, the chamber was sealed with a two-part epoxy (Araldite) and then immediately quenched by placing the chamber on a room temperature surface to obtain the open structure.

Imaging

The samples were imaged using a Nikon Eclipse Ti-E inverted microscope equipped with a digital camera (Grasshopper3, Point Grey Research Inc., Sony IMX174 CMOS sensor) using either a PLAN-APO 20/0.75 dry objective or a PLAN-APO 40/0.75 dry objective. The chambers were attached to a homemade heating/cooling stage consisting of a peltier element and a copper block, which provided homogenous temperature control across the entire sample.

Before heating, the sample was imaged to obtain information on the open structure. Subsequently, the sample was heated to 50°C and left for 20 minutes to achieve a homogenous gas phase of the viruses and gold particles. Afterwards, the samples were quenched to a given temperature below the melt temperature, and time evolution imaging was used to follow the ageing process. Exposure times were kept to a

ARTICLE

minimum and images were taken 20s apart to minimise local heating due gold-NP optical absorption.

Computational Methods

Cord Analysis

The porous structure of the samples was analysed using the chord distribution analysis method[33]. This analysis involves tracing lines (chords) through a binarized image of a biphasic medium, identifying the points at which these lines intersect the boundaries between the gel and the fluid phases. Here we distinguish between pores (p) and aggregate matrix (a)[34]. The distances between neighbouring points represent the length through which the chord passes through a particular domain of one of the two phases. These lengths are tallied in histograms for their respective phases and then normalised to yield probability density functions for the pores ($f_p(r)$) and the aggregate matrix ($f_a(r)$). The probability density functions, which we call the chord distributions, represent the likelihood of finding a chord length r between r and $r+dr$ for a particular phase[35].

Fluorescent microscope images of the aggregates were binarized using ImageJ to find the most appropriate pixel threshold values and then de-noised using standard methods[25]. The resulting images are then analysed by taking chords along horizontal and vertical rows of image pixels, tabulating the respective phase lengths into two histograms.

By inspecting the logarithmic plots of chord distributions against chord length the characteristic length scales of the system can be found. In our porous gels we found a negative exponential relationship[34-36], of the form

$$f_{a,p}(r) \propto \exp(-r/\lambda_{a,p})$$

where $\lambda_{a,p}$ represent the exponential folding length of the chord distribution for the respective phases.

Structure Factor

The structure of the gas phase and the ageing colloidal gel are quantitatively assessed by extracting an effective structure factor $S(q)$ from our epifluorescence microscope images. For a colloidal concentration $c(x,y)$, the structure factor is given by

$$S(q) = \frac{\langle |\tilde{C}(q_x, q_y)|^2 \rangle}{|f(q)|^2},$$

where $\tilde{C}$ denotes the 2D Fourier transform of $c(x,y)$, and $\langle ... \rangle$ denotes the radial average. The form factor $f(q)$ is the Fourier transform of the shape of a single colloid. We assumed that the observed intensity of the image $i(x,y)$ was linearly related to $c(x,y)$, and therefore $S(q)$ could be measured in arbitrary units by replacing $\tilde{C}$ with $\tilde{I}$.[26] We estimated $f(q)$ by taking the Fourier transform of the image of the sample in the gaseous phase such that the structure factor could be expressed as

$$S(q) = \frac{\langle |\tilde{I}(q_x, q_y, t)|^2 \rangle}{\langle |\tilde{I}(q_x, q_y, t=0)|^2 \rangle}.$$

Conclusions

We introduced a new binary system of long filamentous viruses and gold nanoparticles, in which both were functionalized with complementary single-stranded DNA, providing temperature reversible aggregation. The binding rules we established were such that viruses could only bind to gold-NPs while binding between like particles were forbidden. We studied the aggregation of these mixtures as a function of a fast and slow cooling rate, using fluorescence microscopy. The results were analysed in terms of 2D-structure factors and chord-length analysis. Our findings suggest that the structure formation in these NP-virion systems is somewhat different from that in systems of spherical particles. In particular, we find that the wavelength of the dominant density fluctuations hardly depends on the quench depth – in contrast to what the Cahn-Hilliard theory would predict. In addition, we find that the systems that are most deeply quenched, have the largest density inhomogeneities. Whilst this seems logical at first, one should bear in mind that we work in a regime where NP-virion binding is very strong. Hence, at low temperatures, growth of inhomogeneities would seem to be difficult. It seems plausible that the initial instability in the system occurs early in the quench and has the same wavelength for all systems.

As the chord analysis suggests, the systems with a low gold-NP to virus ratio, R_{GV}, can sediment more than the systems with high R_{GV}. A possible explanation is that the low R_{GV} samples `consume' all NPs to bind virions together at an early stage in the phase separation. As a result, the resulting clusters interact only weakly and can sediment well. In contrast, the high R_{GV} clusters will have exposed nano-particles on their surface. These particles will therefore tend to stick to each other and will sediment to form a more open structure. This two–stage phase separation scenario suggests a new method to design the pore structure in disordered nano-particle systems. This behaviour can also be interpreted in terms of an effective coordination number: Due to the large aspect ratio the virions can bind many nanoparticles. Hence, while keeping the gold-NP volume fraction constant but changing the number of available virions to bind to, the effective coordination number of the system changes leading to the different aggregation characteristics.

Acknowledgements

References

1. C. A. Mirkin, R. L. Letsinger, R. C. Mucic and J. J. Storhoff, *Nature*, 1996, **382**, 607-609.
2. A. P. Alivisatos, K. P. Johnsson, X. Peng, T. E. Wilson, C. J. Loweth, M. P. Bruchez and P. G. Schultz, *Nature*, 1996, **382**, 609-611.
3. S. Y. Park, A. K. R. Lytton-Jean, B. Lee, S. Weigand, G. C. Schatz and C. A. Mirkin, *Nature*, 2008, **451**, 553-556.
4. D. Nykypanchuk, M. M. Maye, D. van der Lelie and O. Gang, *Nature*, 2008, **451**, 549-552.
5. E. Auyeung, T. I. Li, A. J. Senesi, A. L. Schmucker, B. C. Pals, M. O. de la Cruz and C. A. Mirkin, *Nature*, 2014, **505**, 73-77.
6. Y. Wang, Y. Wang, X. Zheng, E. Ducrot, J. S. Yodh, M. Weck and D. J. Pine, *Nature communications*, 2015, **6**.
7. N. Geerts and E. Eiser, *Soft Matter*, 2010, **6**, 4647.
8. D. Lukatsky and D. Frenkel, *Physical Review Letters*, 2004, **92**.
9. H. Yin, B. Dong, X. Liu, T. Zhan, L. Shi, J. Zi and E. Yablonovitch, *Proceedings of the National Academy of Sciences*, 2012, **109**, 10798-10801.
10. E. R. Dufresne, H. Noh, V. Saranathan, S. G. J. Mochrie, H. Cao and R. O. Prum, *Soft Matter*, 2009, **5**, 1792-1795.
11. D. S. Wiersma, *Nat Photon*, 2013, **7**, 188-196.
12. J. A. Lewis, *Journal of the American Ceramic Society*, 2000, **83**, 2341-2359.
13. A. Paolella, G. Bertoni, S. Marras, E. Dilena, M. Colombo, M. Prato, A. Riedinger, M. Povia, A. Ansaldo, K. Zaghib, L. Manna and C. George, *Nano letters*, 2014, **14**, 6828-6835.
14. H. Zhang, X. Yu and P. V. Braun, *Nature nanotechnology*, 2011, **6**, 277-281.
15. A. M. Puertas and M. Fuchs, Glasses in Colloidal Systems. Attractive Interactions and Gelation, DOI: arXiv:0810.0681).
16. L. Cipelletti, L. Ramos, S. Manley, E. Pitard, D. A. Weitz, E. E. Pashkovski and M. Johansson, *Faraday Discussions*, 2003, **123**, 237-251.
17. M. E. Cates and M. R. Evans, eds., *Soft and Fragile Matter: Nonequilibrium Dynamics, Metastability and Flow (PBK)*, Institute of Physics Publishing, Bristol and Philadelphia, 2000.
18. W. C. K. Poon, A. D. Pirie and P. N. Pusey, *Faraday Discussions*, 1995, **101**, 65-76.
19. V. Prasad, V. Trappe, A. D. Dinsmore, P. N. Segre, L. Cipelletti and D. A. Weitz, *Faraday Discussions*, 2003, **123**, 1-12.
20. S. Manley, H. M. Wyss, K. Miyazaki, J. C. Conrad, V. Trappe, L. J. Kaufman, D. R. Reichman and D. A. Weitz, *Physical Review Letters*, 2005, **95**, 238302.
21. A. Fierro, E. D. Gado, A. d. Candia and A. Coniglio, *Journal of Statistical Mechanics: Theory and Experiment*, 2008, **2008**, L04002.
22. V. Testard, L. Berthier and W. Kob, *The Journal of Chemical Physics*, 2014, **140**, 164502.
23. G. Foffi, C. D. Michele, F. Sciortino and P. Tartaglia, *Physical Review Letters*, 2005, **94**, 078301.
24. P. J. Lu, E. Zaccarelli, F. Ciulla, A. B. Schofield, F. Sciortino and D. A. Weitz, *Nature*, 2008, **453**, 499-503.
25. F. Varrato, L. Di Michele, M. Belushkin, N. Dorsaz, S. H. Nathan, E. Eiser and G. Foffi, *Proceedings of the National Academy of Sciences*, 2012, DOI: 10.1073/pnas.1214971109.
26. L. Di Michele, F. Varrato, J. Kotar, S. H. Nathan, G. Foffi and E. Eiser, *Nature communications*, 2013, **4**, 2007.
27. L. Di Michele, D. Fiocco, F. Varrato, S. Sastry, E. Eiser and G. Foffi, *Soft Matter*, 2014, **10**, 3633-3648.
28. R. R. Unwin, R. A. Cabanas, T. Yanagishima, T. R. Blower, H. Takahashi, G. P. C. Salmond, J. M. Edwardson, S. Fraden and E. Eiser, *Physical Chemistry Chemical Physics*, 2015, **17**, 8194-8202.
29. L. Di Michele, B. M. Mognetti, T. Yanagishima, P. Varilly, Z. Ruff, D. Frenkel and E. Eiser, *Journal of the American Chemical Society*, 2014, **136**, 6538-6541.
30. F. Sciortino and E. Zaccarelli, *Current Opinion in Solid State and Materials Science*, 2011, **15**, 246-253.
31. D. A. Marvin, *Journal of Molecular Biology*, 1966, **15**, 8-IN4.
32. S. J. Hurst, A. K. R. Lytton-Jean and C. A. Mirkin, *Analytical chemistry*, 2006, **78**, 8313-8318.
33. J. Méring and D. Tchoubar, *Journal of Applied Crystallography*, 1968, **1**, 153-165.
34. P. Levitz, *Advances in Colloid and Interface Science*, 1998, **76–77**, 71-106.
35. P. Levitz and D. Tchoubar, *Journal de Physique I*, 1992, **2**, 771-790.
36. P. Levitz, *Cement and Concrete Research*, 2007, **37**, 351-359.